LDRD Final Report: Energy Conversion Using Chromophore-Functionalized Carbon Nanotubes

Andrew L. Vance, Xinjian Zhou, François Léonard, Bryan M. Wong, Karen L. Krafcik, Tom Zifer, Aaron Katzenmeyer, Alex Kane

 Sandia National Laboratories

LDRD Final Report: Energy Conversion Using Chromophore-Functionalized Carbon Nanotubes

Andrew L. Vance, Bryan M. Wong, Karen L. Krafcik & Tom Zifer
Materials Chemistry Department

Xinjian Zhou, François Léonard, Aaron Katzenmeyer & Alex Kane
Materials Physics Department

Sandia National Laboratories
P.O. Box 969
Livermore, California 94550

Abstract

With the goal of studying the conversion of optical energy to electrical energy at the nanoscale, we developed and tested devices based on single-walled carbon nanotubes functionalized with azobenzene chromophores, where the chromophores serve as photoabsorbers and the nanotube as the electronic read-out. By synthesizing chromophores with specific absorption windows in the visible spectrum and anchoring them to the nanotube surface, we demonstrated the controlled detection of visible light of low intensity in narrow ranges of wavelengths. Our measurements suggested that upon photoabsorption, the chromophores isomerize to give a large change in dipole moment, changing the electrostatic environment of the nanotube. All-electron *ab initio* calculations were used to study the chromophore-nanotube hybrids, and show that the chromophores bind strongly to the nanotubes without disturbing the electronic structure of either species. Calculated values of the dipole moments supported the notion of dipole changes as the optical detection mechanism.

Acknowledgments

Contents

Figures

Nomenclature

DR1   disperse red 1
DR1-PB   disperse red 1 pyrene butyrate
FET   field effect transistor
SWNT   single-walled carbon nanotube
TFT   thin film transistor

1. Introduction

The conversion of optical energy to electrical energy is a topic of great interest, with much research and development invested in conventional materials such as silicon. Due to their unique electronic, optical and mechanical properties, nanomaterials such as nanotubes, quantum dots and nanowires offer much promise for optical energy conversion [1,2]. Amongst nanomaterials, single walled carbon nanotubes (SWNTs) have been discussed for direct photon conversion for several reasons. First, because all of the bandgaps in carbon nanotubes are direct, light absorption can proceed without the intervention of phonons. Second, high speed devices may be possible because electronic transport in nanotubes can have extremely high mobilities and even be quasi-ballistic [3,4]. Third, nanotubes often have low defect density, further eliminating deleterious scattering processes. Fourth, the bandgap of carbon nanotubes is tunable by controlling the nanotube diameter, thus allowing spectrally tunable detection. Despite these advantages, the current state-of-the-art in using nanotubes as photoconductive materials is still in its infancy. While direct photoresponse in individual carbon nanotube devices has been demonstrated, these experiments were done at high light intensities using lasers [5]. Such large light intensities are needed because of the small cross-section for optical absorption from individual nanotubes. In addition, direct conversion schemes using the nanotube as the photoabsorber are hampered by difficulties in controllably synthesizing nanotubes of appropriate chirality. Furthermore, because excitons are strongly bound in nanotubes, large local electric fields are needed to separate the charge carriers [6].

Certain types of chromophores in combination with the nanotube, provide an entirely different photodetection mechanism that does not rely on direct photoabsorption by the nanotube, and this approach uses the advantages of synthetic chemistry that allow the design of molecules with specific optical absorption properties. Recent examples of efforts in this area include functionalization of nanotubes using light-isomerizable spiropyrans [7], porphyrins [8,9] and cyclodextrin [10] to influence the electronic properties of SWNT field effect transistors (FETs). While these systems are intriguing, spiropyrans exhibit limited lifetimes and other molecules like porphyrins work through charge transfer mechanisms that rely on a correct band alignment between the molecular species and the nanotube that may be difficult to achieve. Our work is

based on a different mechanism where photoisomerizable azobenzene-derived chromophores undergo a large change in dipole moment upon light absorption. When non-covalently attached to the surface of a semiconducting carbon nanotube serving as the channel in a FET, this large change in dipole moment leads to a large change in electrostatic potential on the nanotube that impacts its conductance. Thus the carbon nanotube serves as the electronic read-out for the molecular transformations. The general mechanism for this process is illustrated in Figure 1.
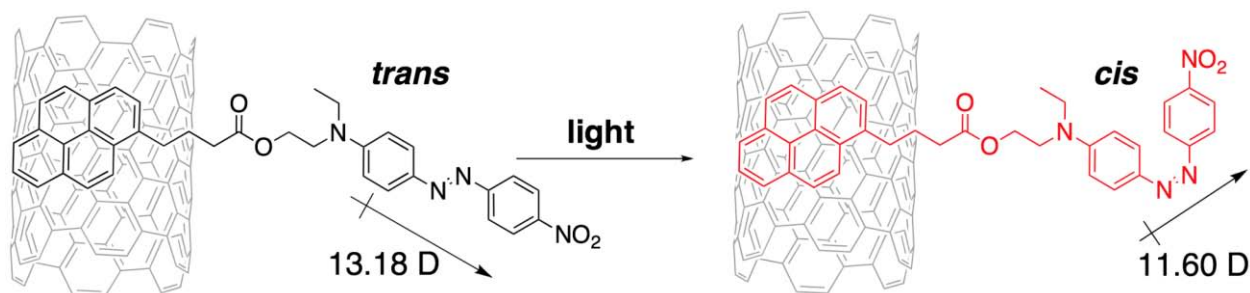
Figure 1. Photoisomerization of azobenzene on SWNT.

In this LDRD project, we studied nanoscale energy conversion by chromophore-nanotube hybrids and developed a fundamental understanding of their behavior. Carbon nanotube devices are clearly a popular area of research; however, there are very few groups studying the conversion of low intensity optical energy into photoresponse, and we were the first to demonstrate photo detection over nearly the entire visible spectrum using SWNT devices. The ability to use light to modulate the conductance of single walled carbon nanotube devices through minimally intrusive, non-covalent modification of the nanotubes could lead to significant advances in areas such as nanoscale electronics, solar energy and photodetectors.

2. Results and Discussion

The chromophore-nanotube hybrid system offers many advantages for photon conversion including high sensitivity and the ability to tune wavelength sensitivity via chemical modifications to the chromophore structure. Building upon the first example of chromophore-nanotube hybrid devices that were sensitive to ultraviolet light [11], we demonstrated color detection using chromophore-nanotube hybrids [12]. (Experimental details are outlined in Appendix A.) Selection of appropriate chromophores allows the nanotube devices to be tuned to respond to specific wavelengths over a wide range from the ultraviolet to the near-infrared.

Synthetic work produced x-ray quality crystals of two compounds [13,14], providing structural data useful to modeling efforts. Figure 2 shows the structures of a series of chromophores synthesized for this project and utilized to tune wavelength sensitivity along with a representation of the non-covalent attachment of pyrene-modified disperse red 1 (DR1-PB)
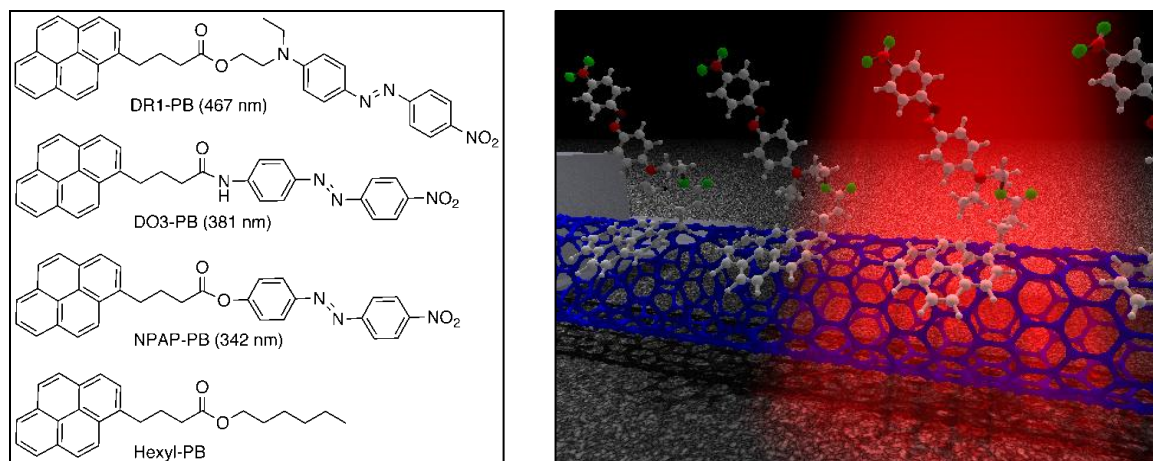
Figure 2. Left - Structures of pyrenebutyric acid functionalized chromophores. The numbers in parentheses are the absorbance maxima of the azobenzene moieties of the dyes. Right - Representation of chromophore-nanotube hybrid with DR1-PB on SWNT.

chromophores to the nanotube surface. This is a unique system in that upon light absorption, the chromophores undergo a trans-to-cis transformation with an associated large change in their dipole moment; this change in dipole moment causes a large change in electrostatic potential around the nanotube. We can thus read-out these molecular transformations by using the
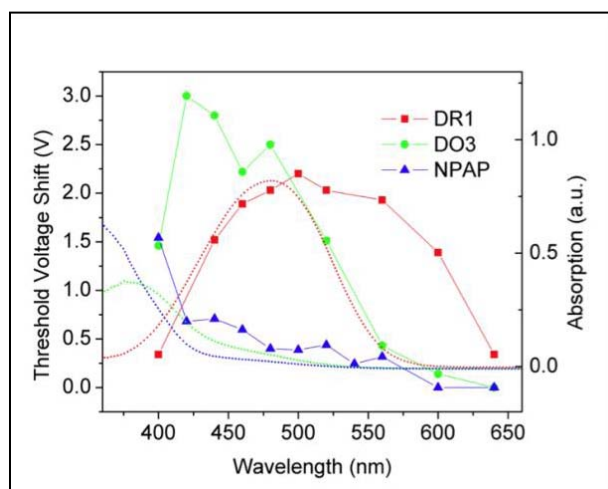
Figure 3. Light-induced threshold voltage shifts of three chromophore-nanotube hybrid FET devices where DR1, DO3 and NPAP are the different chromophores.

nanotube-chromophore hybrids as the channel in a field-effect transistor. Figure 3 shows the response of three SWNT-FET devices where the channel consists of these nanotube-chromophore hybrids. The FET threshold voltage is significantly shifted upon absorption of light by the chromophores, with absorbance maxima ranging from below 400 nm to 500 nm (chromophore absorbance maxima in solution were 342, 381 and 467 nm). The solid lines with data points represent absorption spectra assembled by plotting the device threshold

voltage shift at each wavelength while the dotted lines are the solution spectra for each chromophore. Without the chromophores, the nanotube devices would be unresponsive to these wavelengths at these low light intensities. Furthermore, we have converted optical signal to electrical signal using a single nanotube at light intensities as low as 10 mW/cm^2, about three orders of magnitude less than experiments on direct photoconversion. It should also be noted that the chromophore-nanotube hybrid devices have shown repeatable switching over many cycles with no sign of photobleaching.

To support the hypothesis that the optical detection mechanism is based on a large dipole change in the chromophores, we utilized ab initio quantum calculations to obtain the combined electronic structure of the chromophore-nanotube hybrids. Figure 4 shows a representation of
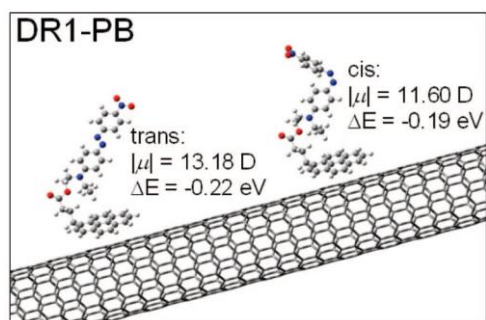
Figure 4. Relaxed atomic structure of DR1-pyrenebutyrate on a (10,0) SWNT, obtained from ab initio calculcations.

one of the systems that we considered, which consists of a high density DR1 monolayer on the surface of a (10,0) nanotube attached through the pyrene linker. Our calculations revealed that the pyrene linker anchors the molecule strongly to the nanotube surface, but in a non-covalent fashion. Indeed, the joint electronic structure is essentially a superposition of the individual electronic structures of the isolated molecules and nanotube, i.e. there is very little hybridization between them.

Furthermore, our calculations showed a very large difference of the molecular dipole moment of more than 1.5 Debye between the trans and cis configurations. Thus, the molecules can be thought of as a gate that is less than 1 nanometer away from the nanotube.

To test the proposed dipole-change mechanism, we performed quantum transport calculations of the nanotube transistor characteristics in the presence of dipoles. (For a detailed discussion of the calculations, see references 11 and 12.) In brief, we used the nonequilibrium Green's function formalism implemented in a tight-binding formalism in conjunction with a Poisson solver to self-consistently calculate the conductance, charge and electrostatic potential in the device. The calculated threshold voltage shift was found to be in excellent agreement with the experiments, thus supporting the dipole change mechanism as the reason for the modulation of the nanotube conductance.

Following on the successful demonstration of light detection using azobenzene chromophores on single nanotube devices, we explored the use of different types of chromophores as well as carbon nanotube thin film transistors (CNT-TFTs) consisting of multiple nanotubes in the device channel. Chromophore-nanotube hybrids using molecules designed to absorb in the upper visible to near-infrared region such as the compound shown in Figure 5 did not exhibit the threshold voltage shifts observed with the azobenzene chromophores. Further study is needed to determine what caused the lack of a measureable light response.
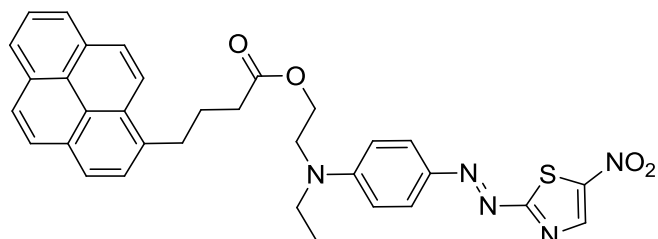
Figure 5. Aminothiazole-derived chromophore with λ_{max} 550 nm.

CNT-TFTs were successfully prepared using various SWNTs including semiconducting nanotube enriched samples prepared via density gradient ultracentrifugation [15]. The TFT-FETs were functionalized with DR1-PB and their response to monochromater-controlled light was measured. Initial results indicate the chromophore did not produce a threshold voltage shift consistent with the absorption spectrum of the chromophore. Possible reasons for the difference between the TFT-FETs and the SWNT-FETs include increased resistance caused by nanotube junctions in the TFTs or insufficient chromophore coverage if the chromophores are not able to attach to all the nanotubes in the thin film. The chromophore signal may also have been masked by changes caused by the photodesorption of water. This is another area where further study is warranted because porphyrin-functionalized CNT-TFTs have been reported to exhibit light sensitivity [9].

Finally, we were interested in examining the use of p-n junction devices functionalized with azobenzene chromophores. These types of devices offer the possibility of photovoltaic response at zero bias. Our initial target was single nanotube p-n junctions prepared using the same Cheaptube SWNTs utilized in the SWNT-FETs. Rather than attempting to chemically alter half of the nanotube to generate n-type behavior as reported by Dai et al. [16], we chose to utilize a dual buried gate architecture where the p-n junction is created electrostatically by varying the two gate voltages. After refining the fabrication process, it was found that reproducibly generating devices that exhibited the desired ambipolarity was a challenge. While devices were

prepared that functioned as p-n junctions, they were not sufficiently stable for use with the chromophores. It has been demonstrated that ideal carbon nanotube p-n junction diodes can be prepared by utilizing a suspended SWNT [17] where the nanotube is not in direct contact with the SiO_2 surface, as in our devices. This device architecture may be required to enable optimized chromophore-nanotube interactions and will be pursued in the future.

3. Conclusions

Through both experimental and theoretical studies, this work showed that SWNTs can transduce the photoabsorption-induced isomerizations of nearby chromophores into electrical signals. By designing chromophores to absorb in a narrow window of the optical spectrum and applying them to SWNT-FETs, sensitive nanoscale color detectors were demonstrated. This system can be used to study fundamental properties of chromophore-nanotube hybrids and to probe molecular transitions. We expect that improvements in the signal transduction will lead to the ability to detect single molecular transformation events, and that molecular engineering can provide detection in other regions of the optical spectrum.

4. References

1. P. Avouris, M. Freitag, V. Perebeinos, Nature Photonics, 2 (2008) 341

2. Q. Cao, J.A. Rogers, Advanced Materials, 21 (2009) 29

3. A. Javey, J. Guo, Q. Wang, M. Lundstrom, H. Dai, Nature, 424 (2003) 654

4. Z. Zhang, X. Liang, S. Wang, K. Yao, Y. Hu, Y. Zhu, Q. Chen, W. Zhou, Y. Li, Y. Yao, J. Zhang, L.-M. Peng, Nano Letters, 7 (2007) 3603

5. M. Freitag, Y. Martin, J.A. Misewich, P. Avouris Nano Letters, 3 (2003) 1067

6. A. Mohite, J.-T. Lin, G. Sumanasekera, B.W. Alphenaar, Nano Letters, 6 (2006), 1369

7. X. Guo, L. Huang, S. O'Brien, P. Kim, C. Nuckolls, Journal of the American Chemical Society, 127 (2005) 15045

8. J.P. Casey, S.M. Bachilo, R.B. Weisman Journal of Materials Chemistry, 18 (2008) 1510

9. D.S. Hecht, R.J.A. Ramirez, M. Briman, E. Artukovic, K.S. Chichak, J.F. Stoddart, G. Grüner, Nano Letters, 6 (2006) 2031

10. Y.L. Zhao, L. Hu, G. Grüner, J.F. Stoddart Journal of the American Chemical Society, 130 (2008) 16996

11. J.M.Simmons, I. In, V.E. Campbell, T.J. Mark, F. Léonard, P. Gopalan, M.A. Eriksson, Physical Review Letters, 98 (2007) 086802

12. X. Zhou, T. Zifer, B.M. Wong, K. Krafcik, F. Léonard, A.L. Vance, Nano Letters, 9 (2009) 1028

13. M.A. Rodriguez, T. Zifer, A.L. Vance, B.M. Wong, F. Léonard, Acta Crystallographica E, E64 (2008) o595

14. M.A. Rodriguez, J.L. Nichol, T. Zifer, A.L. Vance, F. Léonard, Acta Crystallographica E, E64 (2008) o2258

15. M.S. Arnold, A.A. Green, J.F. Hulvat, S.I. Stupp, M.C. Hersam, Nature Nanotechnology, 1 (2006) 60

16. C. Zhou, J. Kong, E. Yenilmez, H. Dai Science, 290 (2000) 1552

17. J.U. Lee Applied Physics Letters, 97 (2005) 073101

Appendix A: Experimental Details

Synthesis

General procedure for esterification/amidation reaction of 1-pyrenebutyric acid with diazobenzene dyes: The dye, 1-pyrenebutyric acid, dicyclohexylcarbodiimide (DCC), and 4-(dimethylamino)pyridine (dmap) were dissolved in anhydrous dichloromethane with stirring. The reaction mixture was stirred until complete (up to 18 hours). The precipitated dicyclohexyl urea was removed by vacuum filtration and the crude product isolated by rotary evaporation of the solvent. Products were purified by recrystallization or column chromatography (silica gel) and characterized as needed by UV/Vis spectrophotometry, FTIR and ^{1}H-NMR spectroscopy, mass spectrometry and x-ray crystallography. Specific examples are described below.

(*E*)-2-(ethyl(4-((4-nitrophenyl)diazenyl)phenyl)amino)ethyl 4-(pyren-1-yl)butanoate (DR1-PB): Using the general procedure above, disperse red 1 (500 mg, 1.59 mmol), 1-pyrenebutryic acid (462 mg, 1.60 mmol), DCC (361 mg, 1.75 mmol) and DMAP (39 mg, 0.32 mmol) were stirred in anhydrous dichloromethane for 18 hours. After filtration of the precipitate and collection of the crude product by rotary evaporation, the red powder was recrystallized from ethyl acetate/ethanol to give a dark red powder (667 mg, 72%). ^{1}H-NMR (500 MHz, CDCl$_3$): δ 8.30 (d, 2H), 8.26 (d, 1H), 8.15 (d, 2H), 8.09 (m, 2H), 8.02-7.92 (m, 7H), 7.82 (d, 1H), 6.80 (d, 2H), 4.28 (t, 2H), 3.63 (t, 2H), 3.49 (q, 2H), 3.36 (t, 2H), 2.45 (t, 2H), 2.20 (m, 2H), 1.21 (t, 3H); UV/Vis: azobenzene λ_{max} 467 nm; FTIR: C=O stretch 1745 cm^{-1}; MS (APCI, positive ion mode) Calcd for C$_{36}$H$_{32}$N$_4$O$_4$: 584.2, Found: 585.4 [M+H]$^+$.

(*E*)-*N*-(4-((4-nitrophenyl)diazenyl)phenyl)-4-(pyren-1-yl)butanamide (DO3-PB): Using the general procedure above, disperse orange 3 (480 mg, 2.0 mmol), 1-pyrenebutryic acid (650 mg, 2.25 mmol), DCC (610 mg, 3.0 mmol) and DMAP (30 mg, 0.2 mmol) were stirred in anhydrous dichloromethane for 18 hours. After filtration of the precipitate and collection of the crude product by rotary evaporation, the orange-red powder was recrystallized from ethyl acetate/ethanol to give a red powder (635 mg, 63 %). ^{1}H-NMR (500 MHz, DMSO-d$_6$): δ 8.42 (d, 2H), 8.35 (d, 2H), 8.13 (m, 2H), 7.88 (m, 7H), 7.74 (d, 2H), 6.70 (d, 2H), 6.50 (bs, 1H), 3.26 (t, 2H), 2.62 (t, 2H), 1.22 (m, 2H); UV/Vis: azobenzene λ_{max} 381 nm; FTIR: C=O stretch 1692 cm^{-1}; MS (APCI, negative ion mode) Calcd for C$_{32}$H$_{24}$N$_4$O$_3$: 512.2, Found: 512.2.

(*E*)-4-((4-nitrophenyl)diazenyl)phenyl 4-(pyren-1-yl)butanoate (NPAP-PB): Using the general procedure above, 4-(4-nitrophenyl)azophenol (490 mg, 2.0 mmol), 1-pyrenebutryic acid (650 mg, 2.25mmol), DCC (540 mg, 2.6 mmol) and DMAP (20 mg, 0.16 mmol) were stirred in anhydrous dichloromethane for 18 hours. After filtration of the precipitate and collection of the crude product by rotary evaporation, the dark red powder was purified on a silica column from ethyl acetate/petroleum ether (50/50) to give a dark red powder (138 mg, 13%). ^{1}H-NMR (500 MHz, DMSO-d$_6$): δ 8.45 (d, 2H), 8.38 (d, 2H), 8.26 (m, 5H), 8.14 (d, 2H), 7.87 (d, 2H), 7.40 (d, 2H), 6.97 (d, 2H), 3.46 (t, 2H), 2.81 (t, 2H), 2.18 (m, 2H); UV/Vis: azobenzene λ_{max} 342 nm; FTIR: C=O stretch 1763 cm^{-1}; MS (APCI, negative ion mode) Calcd for C$_{32}$H$_{23}$N$_3$O$_4$: 513.2, Found: 513.2.

Hexyl 4-(pyren-1-yl)butanoate (hexyl-PB): Using the general procedure above, 1-hexanol (205 mg, 2.0mmol), 1-pyrenebutryic acid (470 mg, 1.6mmol), DCC (390 mg, 1.8mmol) and DMAP (40 mg, 0.3mmol) were stirred in anhydrous dichloromethane for 18 hours. After filtration of the precipitate and collection of the oily crude product by rotary evaporation, the product was purified on a silica gel column with ethyl acetate/petroleum ether (30/70) to give a yellow oil (596 mg, 59%). ^{1}H-NMR (500 MHz, DMSO-d_6): δ 8.37 (d, 1H), 8.26 (t, 2H), 8.22 (m, 2H), 8.12, (d, 2H), 8.05 (t, 1H), 7.93 (d, 1H), 3.98 (t, 2H), 3.33 (t, 2H), 2.45 (t, 2H), 2.02 (t, 2H), 1.51 (t, 2H), 1.22 (m, 6H), 0.81 (t, 3H); FTIR: C=O stretch 1728 cm^{-1}; MS (APCI, positive ion mode) Calcd for $C_{26}H_{28}O_2$: 372.2, Found: 373.3 [M+H]$^+$.

(E)-2-(ethyl(4-((5-nitrothiazol-2-yl)diazenyl)phenyl)amino)ethanol (AT): Sodium nitrite (173 mg, 2.50 mmol) was added to 1.2 mL of conc. sulfuric acid with stirring while cooling on an ice bath. Acetic acid (5.0 mL) was added and the solution stirred over ice as 2-amino-5-nitrothiazole (400 mg, 2.50 mmol) was added in portions. The mixture was stirred over ice for 30 min, giving a dark yellow slurry. 2-(N-ethylanilino)ethanol (413 mg, 2.50 mmol) was dissolved in a mixture of 3.5 mL acetic acid/17.5 mL deionized water at room temperature then cooled on an ice bath before adding to the diazonium slurry. The mixture turned dark brown upon addition of the 2-(N-ethylanilino)ethanol and stirring was continued for another 2.5 hours. The mixture was neutralized by addition of 10% sodium hydroxide solution, producing a dark green precipitate that was collected by vacuum filtration and rinsed with water. The product was dried under vacuum to give a dark powder (188 mg, 23% yield). ^{1}H-NMR (500 MHz, CDCl$_3$): δ 8.60 (s, 1H), 7.94 (2, 2H), 6.82 (d, 2H), 3.95, (t, 2H), 3.69 (t, 2H), 3.64 (q, 2H), 1.30 (t, 3H). UV/Vis: λ_{max} 553 nm.

Carbon Nanotube Preparation and Device Fabrication

Carbon nanotube field effect transistors (FETs) used in this study were prepared with SWNTs purchased from CheapTubes. These tubes were grown using chemical-vapor deposition and have diameters in the range of 0.8-2 nm. SWNTs received in powdered form were ultrasonically dispersed in water with 2 wt% sodium dodecylbenzenesulfonate (SDBS) and purified via ultracentrifugation (36,000 rpm, 2 hours) to yield well-dispersed SWNTs [M.S. Arnold, A.A. Green, J.F. Hulvat, S.I. Stupp, M.C. Hersam, Nature Nanotechnology, 1 (2006) 60]. Silicon wafers with a 100 nm thermal oxide capping layer were treated with (3-aminopropyl)triethoxysilane (APTES) [Y. Huang, X. Duan, Q. Wei, C.M. Lieber, Science, 291 (2001) 630] and incubated with the SWNT solution (The APTES layer provides positive surface charges to the silicon wafers to enhance the attachment of SWNTs, which are wrapped with negatively-charged surfactants). On top of these SWNTs, source-drain electrodes with a typical 2 µm gap were defined with photolithography, and either gold or palladium was e-beam evaporated to make electrical contacts. The density of nanotubes was controlled such that many source-drain gaps are each bridged by a single SWNT. Only semiconducting devices that can be completely shut off by the electrical potential on the highly-doped silicon backgate were selected for chromophore functionalization and testing. In the final step of device fabrication, SWNT FETs were incubated with the chromophore solution for 1 minute and subsequently washed lightly with methanol. The chromophores selectively deposited onto SWNTs via strong non-covalent interactions between nanotube sidewalls and the pyrene linker group of the chromophores [R.J. Chen, Y.G. Zhan, D.W. Wang, H.J. Dai, Journal of the American Chemical Society, 123 (2001) 3838].

Device Testing

Opto-electronic studies were performed on a modified Zeiss optical microscope. Light from a xenon arc lamp was fed into an Acton Spectropro-275 monochromator with a 600 g/mm grating; and the resulting monochromatic light with a 3 nm bandwidth was focused through a long working distance 50X objective to a spot of about 35 μm in diameter, small enough to illuminate only one SWNT FET device. The typical power density of illumination was 100 W/m^2, and the wavelengths ranged from 400 nm to 700 nm. The current of SWNT FETs was measured with an Ithaco 1211 (DL Instruments) preamplifier under a 10 mV DC bias applied between the source and drain electrode.

Theory and Modeling

Geometry optimizations for all cis and trans chromophores were obtained from density functional theory (DFT) calculations using the Slater-Vosko-Wilk-Nusair local density functional15 in conjunction with a 6-31G(d,p) Gaussian basis set. A (10,0) semiconducting SWNT was chosen due to its large enough size to approach those measured experimentally, but small enough to reduce computational costs. Calculations were performed using a one-dimensional supercell along the axis of the nanotube. Since the chromophore molecules are over 5 times longer than the (10,0) unit cell, a large supercell of 12.8 Å along the nanotube axis was chosen, which allows a separation distance of 3.6 Å between adjacent chromophores. Dipole moments of the chromophores were calculated as expectation values of the dipole operator using the Kohn-Sham density matrix. Quantum transport calculations of the nanotube transistor characteristics in the presence of dipoles were performed using the nonequilibrium Green's function formalism implemented in a tight-binding formalism in conjunction with a Poisson solver to self-consistently calculate the conductance, charge and electrostatic potential in the device (details in reference 11).

Distribution

| 1 | MS0899 | Technical Library | 9536 (electronic copy) |
| 1 | MS0123 | D. Chavez, LDRD Office | 1011 (electronic copy) |